Nanotemplated platinum fuel cell catalysts and copper-tin lithium battery anode materials for microenergy devices.

J.F. Rohan[*,1], M. Hasan and N. Holubowitch.

Abstract.

Nanotemplated materials have significant potential for applications in energy conversion and storage devices due to their unique physical properties. Nanostructured materials provide additional electrode surface area beneficial for energy conversion or storage applications with short path lengths for electronic and ionic transport and thus the possibility of higher reaction rates. We report on the use of controlled growth of metal and alloy electrodeposited templated nanostructures for energy applications. Anodic aluminium oxide templates fabricated on Si for energy materials integration with electronic devices and their use for fuel cell and battery materials deposition is discussed. Nanostructured Pt anode catalysts for methanol fuel cells are shown. Templated CuSn alloy anodes that possess high capacity retention with cycling for lithium microbattery integration are also presented.

Keywords: Electrodeposition, nanotemplate, fuel cell anode catalysts, battery anodes.

* Tel.: +353 21 4904224, Fax.: +35321 4270271
james.rohan@tyndall.ie
[1] ISE Member

1. Introduction.

Integrated electronic and energy devices for advanced micro and nanosystems technology require the development and optimisation of energy sources with increased performance per unit substrate area. Thin film microbatteries were first introduced in the mid 1990's with moderate energy capacity [1,2] and operation rates. They are based on vacuum-deposited planar thin film format with micron scale active materials. Examples of routes to improve the microenergy systems by structuring of the active materials have been reviewed and materials processing routes continue to be described and implemented for 3D microbattery fabrication [3-5]. Nanotemplated materials have significant potential for applications in energy conversion and storage devices due to their unique physical properties. Nanostructured materials provide additional electrode surface area beneficial for these applications and they lead to short path lengths for electronic and ionic transport and thus the possibility of higher reaction rates [3,6,7]. Control of the active materials at the nanoscale is required to minimise the catalyst dimension for fuel cell materials or active battery materials particularly where solid-state ionic diffusion is a limiting factor in the electrode reactions.

Early attempts to develop nanotemplated materials focused on the use of polymer templates [8-10] that could be pretreated to enable active materials deposition within the pores. Subsequently, higher pore density anodic aluminium oxide (AAO) substrates have been developed [11] with higher pore density than the track etched polycarbonate templates (10^9 to 10^{11} pores/cm^2 by comparison with 10^8 pores/cm^2) and the possibility to form pores with smaller diameter (to low nm level) vertically aligned for more

ordered channels and active materials. AAO processing on Si has been investigated [12-14] and is under development as a means to optimise the materials nanotemplating and integration of passive devices with silicon technology [3,15,16]. A particular issue with the template fabrication on Si is the need to have a conducting layer under the aluminium and to which contact must be made for subsequent nanowire deposition in high density and with sufficient structural integrity to remain well adhered following the template removal step.

In this work, we will report on the use of controlled nanotemplate fabrication on Si for microenergy systems integration with electronic devices. The electrodeposition of metal and alloy active materials in templates for energy applications is then described. Direct methanol fuel cell (DMFC) anode catalyst fabrication on Si will be shown and discussed. Templated CuSn alloy materials that possess high capacity retention with cycling for lithium microbattery integration will also be presented. The materials nanostructures are characterised by SEM and XRD and the electrochemical performance analysed.

2. Experimental.

Al films (2.7 μm thick) were sputter deposited on Au/Cr (100 and 20 nm thickness, respectively) on Si wafer substrates and a controlled anodisation created porous AAO templates presenting a well-ordered honeycomb structure. The 2-step anodisation was carried out by first anodising at 21 ^{o}C and 40 V in 0.4 mol dm^{-3} oxalic acid for 5 minutes. The nascent porous alumina template was etched away in 5 wt% H_3PO_4 at 40

°C for 20 minutes and a second anodisation performed for 30 minutes at 21 ^{o}C and 40 V in 0.4 mol dm^{-3} oxalic acid. Finally, treatment for 10 minutes at 40 °C in 5 wt% H_3PO_4 was used for removal of the aluminium oxide barrier layer and widening of the pore diameter. The SEM image of figure 1 (a) is for the porous alumina after the first step anodisation and phosphoric acid. Figure 1 (b) is the AAO following the second anodisation and pore widening. This method generates pores ca. 3 μm in length with 60-70 nm average diameters. The 2-step anodisation process could not be used on Al films 2 μm or less in thickness, as the pore widening step led to pore wall dissolution and a loss of structural integrity.

Platinum was plated from a commercial Metakem Pt-DNS bath (pH 2.5) at 40 °C by a pulsed deposition method. Alternating pulses of -10 mA/cm^2 and +1 mA/cm^2 for 0.1 s each for 3000 cycles were applied. The pulse deposition method helps to replenish Pt ions at the plating interface and reduce hydrogen evolution that inhibits nanowire growth. Finally, the AAO template was removed in 0.5 mol dm^{-3} KOH for 15 minutes.

CuSn deposition was achieved using a bath prepared by mixing 0.26 mol dm^{-3} $Sn(O_3SCH_3)_2.4H_2O$ (Sigma Aldrich, 50 % wt as water content) and 0.026 mol dm^{-3} $Cu(O_3SCH_3)_2.4H_2O$ in 1 mol dm^{-3} CH_3SO_3H aqueous solution. Polyethylene glycol (PEG) (300 ppm) (SigmaUltra, mol. wt. 3350, powder) and Cl^- (50 ppm) as NaCl (BDH, analytical reagent grade) were also added to the electrolyte to suppress the Cu deposition with respect to Sn. Commercially available (Whatman Anodisc® 25) AAO were used for analysis of templated CuSn deposits. The template is 60 μm thick and pore diameter is 200 to 300 nm. Ni was evaporated onto one side to act as the substrate

for CuSn deposition. The backside was then protected so that deposition occurred through the pores only towards the anode. The electrodeposition of templated CuSn was carried out at constant current and room temperature with a slow convection of the electrolyte. A constant current 20 mA was applied using a CHI 660C potentiostat in a two electrode set up with platinised Ti mesh as the anode. After deposition the AAO was dissolved in 0.75 mol dm^{-3} NaOH (Sigma Aldrich) solution for 50 minutes, washed with water and dried in air.

Elemental analysis was performed with an energy dispersive x-ray spectrometry (EDS) (Hitachi S4000 and FEI Nova 630 Nano-SEM coupled with Princeton Gamma technology at 15 kV). The microstructure of the CuSn deposits was analysed by scanning electron microscopy (SEM) (FEI Nova 630 Nano-SEM and Hitachi S-4000 at 20 kV) and characterised by X-ray powder diffraction (Phillips PW3710-MPD with Cu Kα radiation, l = 0.154056 nm, at 40 kV (35 mA) and data was analysed using Philips X'pert XRD software).

The Li capacity test was performed by cyclic voltammetry and constant current experiments using the CH Instruments 660C potentiostat and a three-electrode set-up. The electrolyte consisted of 1 mol dm^{-3} $LiPF_6$ in ethylene carbonate (EC)/diethyl carbonate (DEC) (1:1, in volume) purchased from Sigma-Aldrich. Lithium foil of 0.25 mm thickness (Aldrich) served as counter and reference electrodes. The cell was assembled in an argon-filled glove box (M. Braun Inertgas-System GmbH, Germany, where O_2 and H_2O were maintained at 0.1 ppm level. The capacity values were

measured by calculating the total Coulombic charge during Li-ion insertion and extraction for the charge and discharge curves, respectively.

3. Results and Discussion.

3.1 Nanotemplated fuel cell anode catalysts on Si.

Conventional fuel cell electrodes involve a large number of electron transfer interfaces, increasing resistance and reducing the operating output potential difference for the entire cell. The resistance, or ohmic losses, are well known to be a major limitation of DMFCs at the typical operational cell potential [17] and their minimization is crucial in cell design. In that work unsupported Pt nanowires were used which reduce the ohmic losses by having fewer electron transfer interfaces. Their procedure utilized polycarbonate templates to grow 6 μm long, 50 nm diameter wires (aspect ratio = 120). With their design, however, Pt loading had to be sufficiently high (ca. 3 mg/cm^2) in order to surpass the current efficiency of conventional carbon based electrodes. In this laboratory we have demonstrated that a confined AAO templated composite with carbon nanotubes codeposited in the plating step led to improved performance for methanol oxidation in terms of decreased overpotential for reaction, increased current capability and more tolerance to or minimised influence of reaction byproducts [18].

In the current work in-house AAO template fabrication processes were optimised on Si substrates with a metal underlayer to provide electrical contact and physical support,

since commercially available templates are fragile and nonconductive. Also, smaller pore openings than those of commercial templates are achievable by this method. AAO templates with these characteristics allow for the integration on Si of materials such as catalyst electrodes in micro-direct methanol fuel cells. The porous templates serve as nanoscale scaffolding for the electrodeposition of nanowire arrays for fuel cell catalysts.

Subsequently, Pt metal was electrodeposited into the pores of the template, adhering to the underlying metal layer. Finally, the template was removed in NaOH revealing an array of free-standing Pt nanowires up to 3 μm in length and 60 nm average diameter. A SEM image of a Pt nanowire array generated by the process developed is shown in figure 2. This shows that the barrier layer between the AAO and the metal contact underlayer was removed and the Pt can be deposited with high efficiency on the Si based substrate. The approximate Pt loading for 60 nm diameter, 3 μm long Pt nanowires is 1.8 mg/cm^2.

An example of methanol oxidation activity for such a Pt nanotemplated catalyst fabricated on a Si substrate (~ 1 μm in length and with 60 nm diameter nanowires) is shown in figure 3 where the wire length was decreased to ensure the Pt loading was approximately 0.6 mg/cm^2. It can be seen that the activity is considerably enhanced for the nanowire composite by comparison with the planar substrate on Si. It is also clear that the mass activity or peak current for the methanol oxidation reaction is ~15 mA/mg which is equivalent to the data reported previously (where the increased sweep rate, 50 mV/s and methanol concentration, 2 mol dm^{-3} of that work are taken into consideration) for Pt nanowires fabricated in polycarbonate templates but then dislodged and pasted as

an ink on a conducting substrate or typical Pt nanoparticles dispersed on high surface area carbon [17]. In this work, the nanotemplated wires can be utilised as fabricated on the Si based substrate. Further development of this processing is underway to integrate carbon nanotubes in the smaller diameter pore of the AAO fabricated on Si by comparison with the commercial Whatman AAO discussed in our previous work [18].

3.2 Nanotemplated CuSn lithium battery anodes.

The optimisation of Li-ion battery materials requires the simultaneous improvement in nanostructuring to permit ionic and electronic transport within the electrode while maintaining the quantity of active material per unit area. This differs from the requirements of fuel cells where we seek to minimise the quantity of active catalyst material. Nanotemplated electrodes processed in AAO with sub 100 nm diameters can meet the battery electrode requirements by maintaining the quantity of active material per unit footprint given that aspect ratios of 20 and greater can be achieved. However, to extract performance uniformly from the active material along the length of the nanostructures it is necessary to have sufficient electronic conductivity in the active material or support [19].

Cu is an ideal support material in that it is low cost and has high electrical conductivity. We have recently shown [20] that Cu nanowires or nanotubes can be readily fabricated in AAO with high aspect ratio depending on the additive content of a typical copper sulphate based bath. It is possible to modify the outer surface of the Cu conductor by post processing to yield lithium battery active materials. Cu nanotubes with the external

surface of the nanotubes converted to active lithium battery anode (Cu_2O) material can maintain lithium cycling at high rates and with low capacity loss while the fully converted nanostructure suffered dramatic loss of capacity within 10 cycles [21]. This has been attributed to the isolation of active materials on cycling when a sufficient electrical support was not included in the high aspect ratio active material. While the oxide anodes exhibited good mechanical stability and cyclability the potential range over which the Li reactions occur extends up to 2.5 V vs Li/Li^+ and as such limits their applicability as battery anodes. In recent years, Sn-based intermetallic compounds Sn_xM_y (M = Li^+ inactive matrix) have been studied as promising anode materials. These include Cu_6Sn_5 [22-25], $Ni_xCu_{6-x}Sn_5$ [26], Ni-Sn [27-30] and Fe-Sn [31,32] due in particular to the large reversible specific capacity and the acceptable rate capability. The concept of introducing an inactive matrix to anode materials was proposed by Huggins et al [33].

Among the above different alloying combinations, Cu_6Sn_5 is a prospective anode material mainly because of strong inter-structural relationship between the parent Cu_6Sn_5 compound and its lithiated product [34]. Kepler et al. proposed that Li^+ insertion into beta-phase η-Cu_6Sn_5 produces an intermediate phase $Li_xCu_6Sn_5$ ($x \approx 13$), and the parent intermetallic compound Cu_6Sn_5 reforms in the reverse reaction, when Li^+ is extracted completely [22]. They also reported that Cu_6Sn_5 reacts reversibly with Li to deliver an initial discharge capacity of 358 mA h g^{-1} based on structural similarity with the highest lithiated phase $Li_{2.17}CuSn_{0.83}$ (or $Li_{13}Cu_6Sn_5$). Larcher et al. reached a similar result on the Li^+ insertion and de-insertion mechanism of Cu_6Sn_5, with $Li_{4.4}Sn$ reported to be an additional phase at the cathodic potentials at 0.0 V vs Li/Li^+ [35].

They have illustrated that inserted Li^+ resides at the hexagonal lattice in the initial transitional $Li_xCu_6Sn_5$ phase (NiAs-type structure, $P6_3/mmc$) for $0 < x < 13$ of the Cu_6Sn_5, which is similar to an iso-structure of the cubic symmetry phase Li_2CuSn /$Li_{13}Cu_6Sn_5$ (Cu_2MnAl-type, Fm/3m). In the second stage of lithiation, $Li_{13}Cu_6Sn_5$ breaks down into Sn and Cu, from which Sn provides Li capacity as the highest lithiated phase $Li_{4.4}Sn$, and Cu diffuses into the solid as nanoscale grains. Although, $Li_{4.4}Sn$ has been identified in the highest lithiated product, identification of the precise composition is quite difficult. Choi et al. have analysed the composition with the help of transmission electron microscopy (TEM) as $Li_{3.5}Sn$, at the potential 0.01 V vs Li/Li^+, close to the cut-off potential of 0 V vs Li/Li^+ [36].

Cu_6Sn_5 alloy has been synthesised by several methods, such as mechanical processes (e.g., direct high temperature synthesis, high-energy ball milling procedure) [23, 37] and chemical reduction methods [38-40]. Recently, a composite Cu_6Sn_5-graphite anode has been synthesised through a ball milling process, and a subsequent carbon coating is given by pyrolysis of polyvinyl chloride (PVC) [41]. This new type of carbon coated Cu_6Sn_5-graphite composite anode material showed excellent cycle performance with a capacity fade of less than 5% and reversible capacity as high as 200 mA h g^{-1}. However, the practical application of such materials in 3D microbattery formats is limited due firstly to the increased weight and ohmic resistance of the cell, as the electrode preparation involves the use of different binding and additive materials and secondly, pasting of Cu_6Sn_5-graphite composite slurry on 3D substrates is not readily achieved.

For Li-ion rechargeable microbatteries, 3D structuring of the electrode is widely accepted as the means to increase the current drain capabilities. Therefore, electrodeposition is considered superior to other methods by virtue of substrate design flexibility, micro- to nano-level deposition, and production cost. Beattie et al. have synthesised Cu-Sn alloy on Ni substrate by pulsed electrodeposition, containing Cu and Sn in a common bath [25]. Nevertheless, they concluded that it is difficult to control the expected alloying composition in nanostructures by the pulsed electrodeposition technique. In this work, Cu_6Sn_5 has been synthesised directly by electrodeposition from a single, high efficiency methanesulfonate plating bath, where Cu and Sn salts are mixed as sulphonate in a 1 : 10 molar ratio. The electrochemical properties of the Cu methanesulfonate bath have been discussed in a recent paper [42]. The exact stoichiometry and surface morphology of the Cu_6Sn_5 deposits are influenced by cathodic current densities, bath compositions, additives and temperature of solution.

Figures 4 (a) and (b) are SEM images of the homogeneous and ordered growth of the template prepared Cu_6Sn_5 alloy deposited in Whatman AAO templates. The elemental analysis of the deposits using EDS shows the presence of Cu and Sn with an atomic ratio of Cu to Sn of 1.13 that complies with the composition of η-Cu_6Sn_5 (atomic ratio = 1.128). The XRD patterns of the electrodeposited Cu_6Sn_5 are shown in figure 5, which are well matched with the desired material [48, 50]. A small peak corresponding to SnO_2 formation may be associated with local pH variation inside the template pores during electrodeposition [30].

The deposit weight of Cu_6Sn_5 nanowires is estimated from the height, diameter and number of nanowires (10^9 pores/cm^2 in Whatman AAO membranes) in a 3 cm^2 AAO template, and assuming the Cu_6Sn_5 density of 8.28 g/cm^3. For example, a Cu_6Sn_5 nanowire with a measured height of 5 μm and diameter of 250 nm, the total weight of the deposits is calculated to be 6.06 g/3cm^2. The electrochemical performance of 1D Cu_6Sn_5 nanowires was studied by cyclic voltammetry. Figure 6 is a charge-discharge curve of Li test in Cu_6Sn_5 nanowires measured by cyclic voltammetry. The first charge and discharge capacity of the nanowires are 325 mA h g^{-1} and 241 mA h g^{-1}, respectively, with an irreversible capacity loss of 84 mA h g^{-1}. The specific charging capacity of the first cycle is close to the theoretical Li storage capacity of Cu_6Sn_5 corresponding to the formation of a fully lithiated composition $Li_{2.17}CuSn_{0.83}$ (358 mA h g^{-1}) [22].

The irreversible capacity during the first cycle is associated with the formation of a small amount of non-transferable lithiated transition phase (e.g., $Li_{2-x}CuSn$) [35] and possible side reactions with the electrolyte due to the presence of a small amount of SnO_2 [44] as confirmed by the XRD above. It can also be seen from figure 6 that the charge values for Li^+ insertion and extraction, respectively, are very similar from the third cycles, implying that electrode exhibits reversible capacity. The charge-discharge capacity is stabilised at 175 to 200 mA h g^{-1} from the third cycle with no significant deterioration. The obtained results imply that a topotactic reaction mechanism for Li^+ insertion/extraction is established with suppressed irreversible capacity loss due to the non-transferable lithiated transition phase and oxide impurities [35,37.41].

Figure 7 shows the cyclic voltammograms of Cu_6Sn_5 templated wires with a deposit height of 5 μm (deposited at 20 mA for 6 minutes and equivalent weight of 6.06 g/3cm^2). The minimal deterioration in lithium capacity on cycling from the third cycle is clearly observed. The high cycling efficiencies of the self-supported Cu_6Sn_5 nanowire electrodes may be attributed to the short Li^+ and e^- transport lengths, easy electrolyte access to the active material through the increased electrolytic contact area and good electronic conductivity of the Cu based alloy. The electrode retains structural integrity leading to increased cyclability.

4. Conclusions.

Nanotemplated materials for energy conversion and storage devices have been discussed. The development of a process for AAO formation on Si substrates to facilitate microenergy source integration with electronic devices has been described. Infilling of these templates with Pt nanowires has been achieved. The nanowire catalysts achieved comparable activity to previously reported nanowires fabricated in templates but then dispersed on a conducting substrate and typical Pt nanoparticles distributed on high surface area carbon supports. The process discussed here utilises the nanotemplated catalysts fabricated on Si to assist with integrated energy sources for electronic applications.

Commercial AAO templates were also utilised for lithium microbattery materials development. The CuSn alloy deposited showed enhanced capacity retention after the

first two cycles indicating a topotactic reaction mechanism for Li^+ insertion and extraction with suppressed irreversible capacity loss due to the non-transferable lithiated transition phase and oxide impurities. The templated CuSn alloy anodes possess high capacity retention with cycling for potential lithium microbattery integration on Si substrates.

Acknowledgements.

This work was supported by the Enterprise Ireland under the following research projects CFTD/05/IT/317, CFTD/07/325.

References

[1]. J.B. Bates, N.J. Dudney, D.C. Lubben, G.R. Gruzalski, B.S. Kwak, X. Yu, R.A. Zuhr, J. Power Sources 54 (1995) 58

[2]. S.D. Jones, J.R. Akridge, J. Power Sources 54 (1995) 63

[3]. J.W. Long, B. Dunn, D.R. Rolison, H.S. White, Chem. Rev. 104 (2004) 4463.

[4]. D. Golodnitsky, V. Yufit, M. Nathan, I. Shechtman, T. Ripenbein, E. Strauss, S. Menkin, E. Peled, J. Power Sources 153 (2006) 281.

[5]. L. Baggetto, R.A.H. Niessen, F. Roozeboom, P.H.L. Notten, Adv. Funct. Mater., 18 (2008).1057

[6]. C. R. Sides, C. R. Martin, *Nanomaterials in Li-Ion Battery Electrode Design, Modern Aspects of Electrochemistry, no. 40,* R. E. White, Editor, p. 75, Springer, New York (2007)

[7]. J. Baxter, Z. Bian, G. Chen, D. Danielson, M.S. Dresselhaus, A.G. Fedorov, T.S. Fisher, C.W. Jones, E. Maginn, U. Kortshagen, A. Manthiram, A. Nozik, D.R. Rolison, T. Sands, L. Shi, D. Sholl, Y. Wu, Energy Environ. Sci., 2 (2009) 559.

[8]. C. R. Martin, Adv. Mater. 3 (1991) 457,

[9]. J. C. Hulteen, C. R. Martin, J. Mater. Chem. 7 (1997) 1075,

[10]. S. A. Sapp, B.B. Lakshmi, C. R. Martin, Adv. Mater. 12 (1999) 402.

[11]. H. Masuda, K. Fukuda, Science 268 (1995) 1466

[12]. S. Shingubara, O. Okino, Y. Sayama, H. Sakaue, T. Takahagi, Solid-State Electronics 43 (1999) 1143

[13]. D. Crouse, Y.H. Lo, A.E. Miller, M. Crouse, Appl. Phys. Lett. 76 (2000) 49

[14]. N.V. Myung, J. Lim, J-P. Fleurial, M. Yun, W. West, D. Choi, Nanotechnology, 15 (2004) 833

[15]. J-H. Kim, S. Khanal, M. Islam, A. Khatri, D. Choi, Electrochem. Commun., 10 (2008) 1688

[16]. F. Cheng, Z. Tao, J. Liang, J. Chen, Chem. Mater. 20 (2008) 667

[17]. S.M. Choi, J.H. Kim, J.Y. Jung, E.Y. Yoon, W.B. Kim, Electrochim. Acta, 58 (2008) 5804

[18]. L.C. Nagle, J.F. Rohan, J. Power Sources, 185 (2008) 411

[19]. R.W. Hart, H.S. White, B. Dunn, D.R. Rolison, Electrochem. Commun., 5 (2003) 120

[20]. T. Chowdhury, D.P. Casey, J.F. Rohan, Electrochem. Commun., 11 (2009) 1203

[21]. M. Hasan, T. Chowdhury, J.F. Rohan, J. Electrochem. Soc. 157 (2010) A682

[22]. K.D. Kepler, J.T. Vaughey, M.M. Thackeray, Electrochem. Solid-State Lett., 2 (1999) 307.

[23]. G.X. Wang, L. Sun, D.H. Bradhurst, S.X. Dou, H.K. Liu, J. Alloys Compd., 299 (2000) L12.

[24]. Y. Xia, T. Sakai, T. Fujieda, M. Wada, H. Yoshinaga, J. Electrochem. Soc., 148 (2001) 471.

[25]. S.D. Beattie, J. R. Dahn, J. Electrochem. Soc., 150 (2003) A894.

[26]. Zhang, Y. Zhang, X. Zhang, Y. Xia, J. Power Sources, 167 (2007) 171

[27]. G.M. Ehrlich, C. Durand, X. Chen, T.A. Hugener, F. Spiess, S.L. Suib, J. Electrochem. Soc., 147 (2000) 886.

[28]. H. Mukaido, T. Sumi, T. Yokoshima, T. Momma, T. Osaka, Electrochem. Solid-State Lett., 6 (2003) A218.

[29]. H. Mukaibo, T. Momma, T. Osaka, J. Power Sources, 146 (2005) 457.

[30]. H. Mukaibo, T. Momma, M. Mohamedi, T. Osaka, J. Electrochem. Soc., 152 (2005) A560.

[31]. O. Mao, R.L. Turner, I.A Courtney, B.D. Fredericksen, M.I Buckett, L.J. Krause, J.R. Dahn, Electrochem. Solid-State Lett., 2 (1999) 3.

[32]. O. Mao, J.R. Dahn, J. Electrochem. Soc., 146 (1999) 414.

[33]. J. Wang, I.D. Raistrick, R.A. Huggins, J. Electrochem. Soc., 133 (1986) 457.

[34]. M.M. Thackeray, J.T. Vaughey, C.S. Johnson, A.J. Kropf, R. Benedek, L.M.L Fransson, K. Edstrom, J. Power Sources, 113 (2003) 124.

[35]. D. Larcher, L.Y. Beaulieu, D.D. MacNeil, J.R. Dahn, J. Electrochem. Soc., 147 (2000) 1658.

[36]. W. Choi, J.Y. Lee, H.S. Lim, Electrochem. Commun., 6 (2004) 816.

[37]. L. Fransson, E. Nordstrom, K. Edstrom, L. Haggstrom, J.T. Vaughey, M.M. Thackeray, J. Electrochem. Soc., 149 (2002) A736.

[38]. Wolfenstine, S. Campos, D. Foster, J. Read, W.K. Behl, J. Power Sources, 109 (2002) 230.

[39]. D.G. Kim, H. Kim, H.-J. Sohn, T. Kang, J. Power Sources, 104 (2002) 221.

[40]. F. Wang, M. Zhao, X. Song, J. Alloys Compd., 439 (2007) 249.

[41]. N. Jayaprakash, N.Kalaiselvi C.H. Doh, J. Appl. Electrochem., 37 (2007) 567.

[42]. M. Hasan, J.F. Rohan, J. Electrochem. Soc., 157 (2010) 278.

[43]. D.G. Kim, H. Kim, H.-J. Sohn, T. Kang, J. Power Sources, 104 (2002) 221.

[44]. C. Kim, M. Noh, M. Choi, J. Cho, B. Park, Chem. Mater., 17 (2005) 3297

Figure captions.

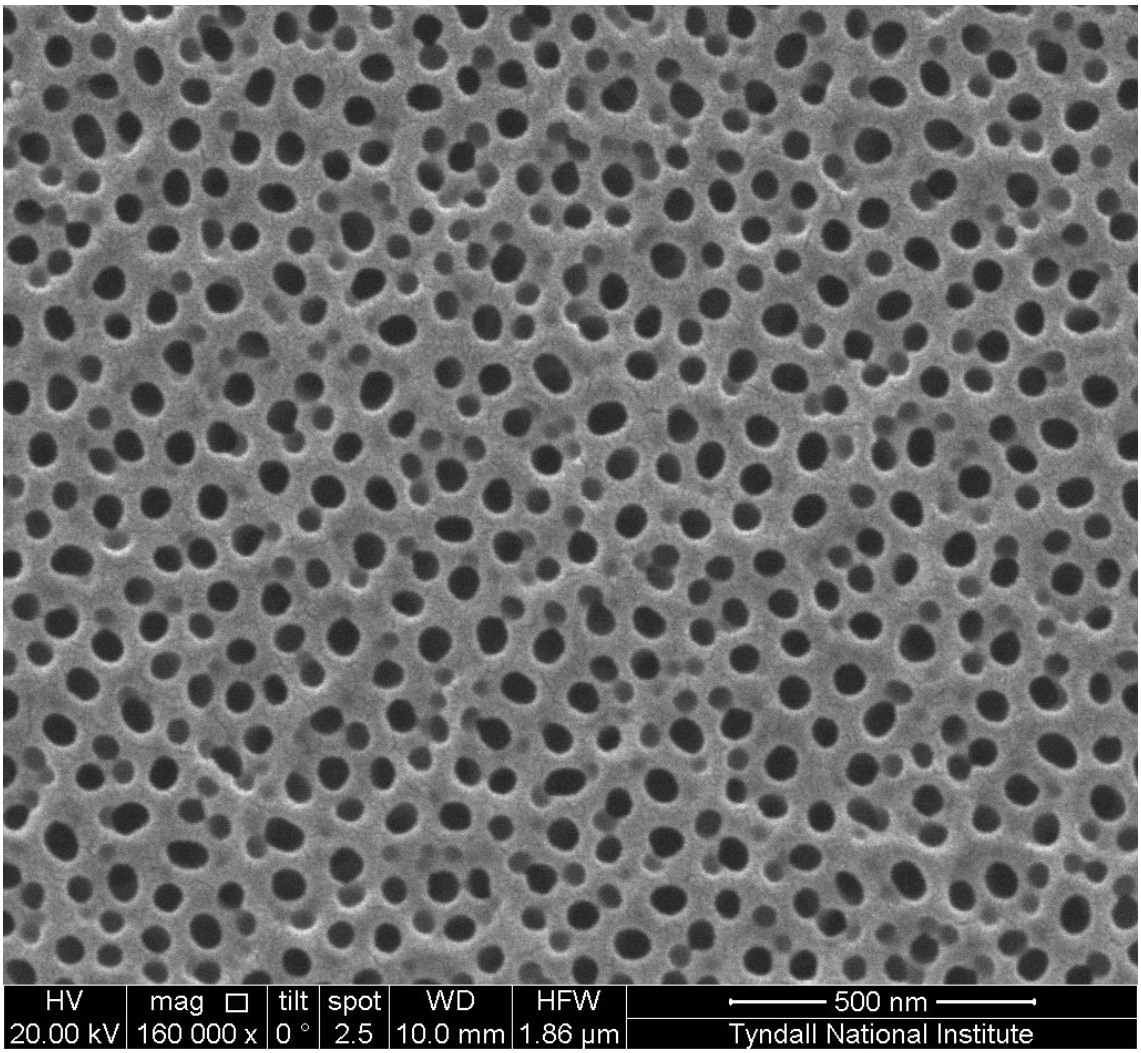

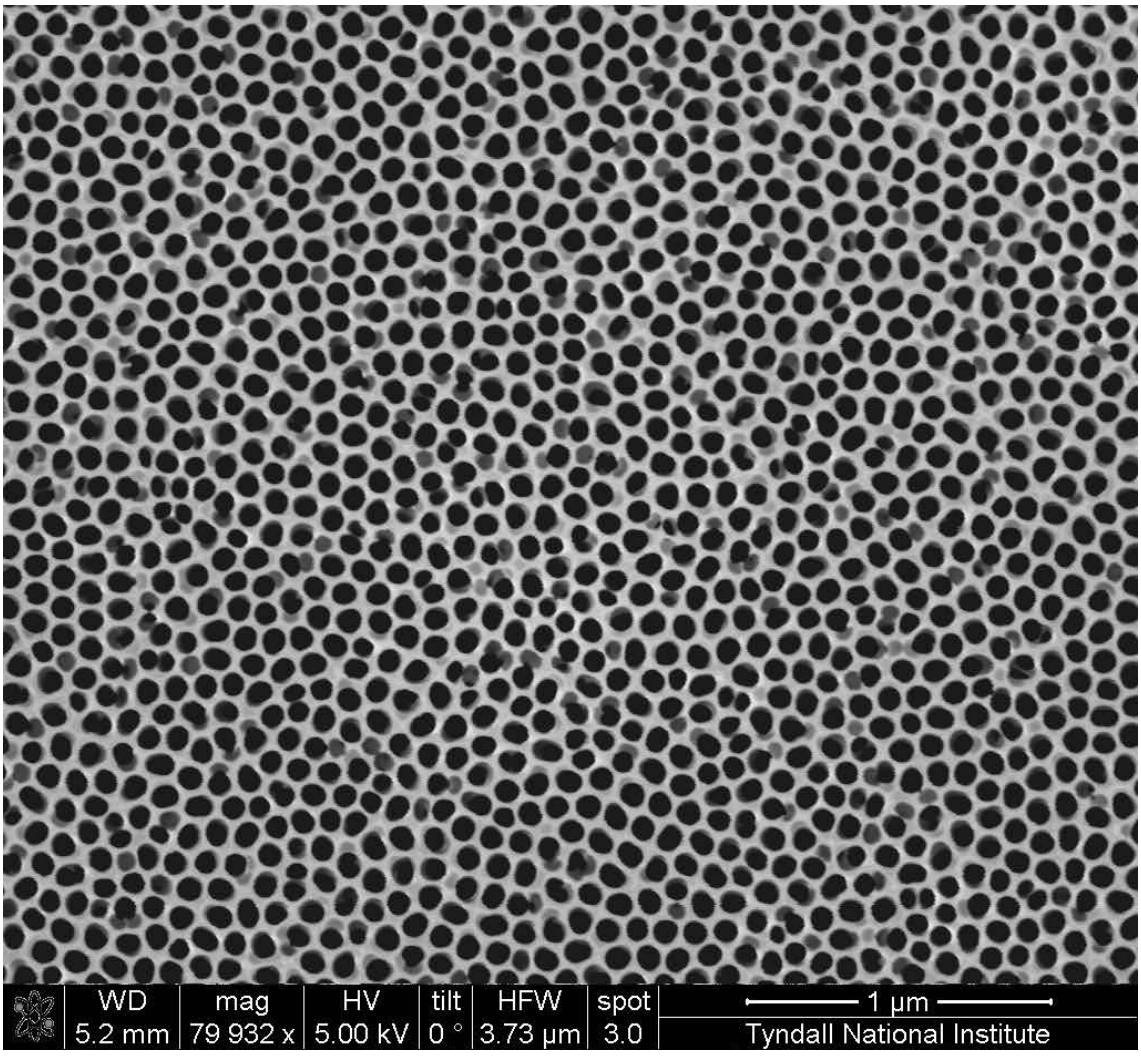

Figure 1(a) SEM image of a thin film sputtered Al film after first step anodisation in 0.4 mol dm^{-3} oxalic acid at 21^{o}C. (b) AAO template formed on Si after a second anodisation performed for 30 minutes at 21 ^{o}C and 40 V in 0.4 mol dm^{-3} oxalic acid and a final etch for 10 minutes at 40 °C in 5 wt.% H_3PO_4.

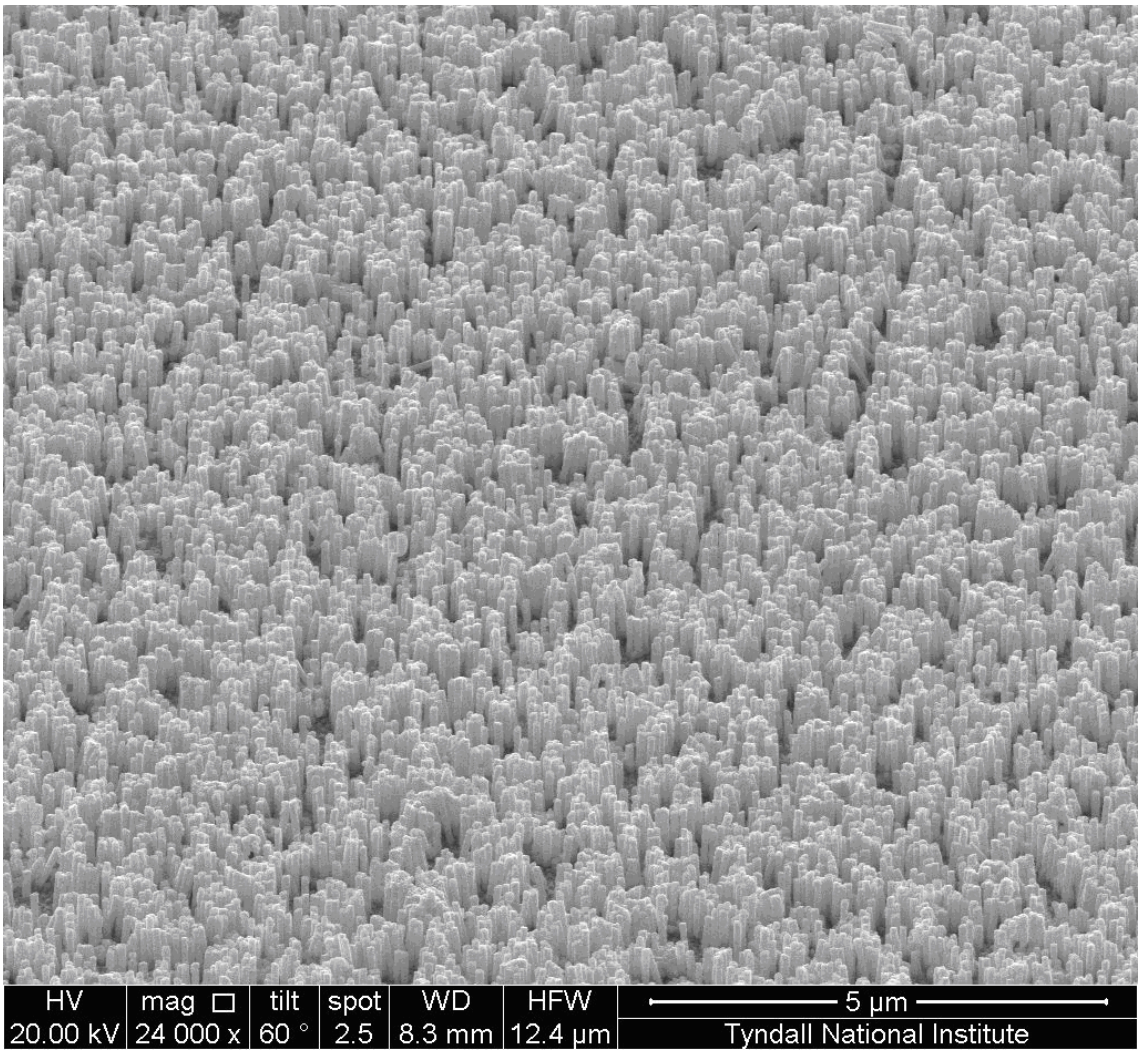

Figure 2. SEM image of an array of Pt nanowires formed in AAO on Si.

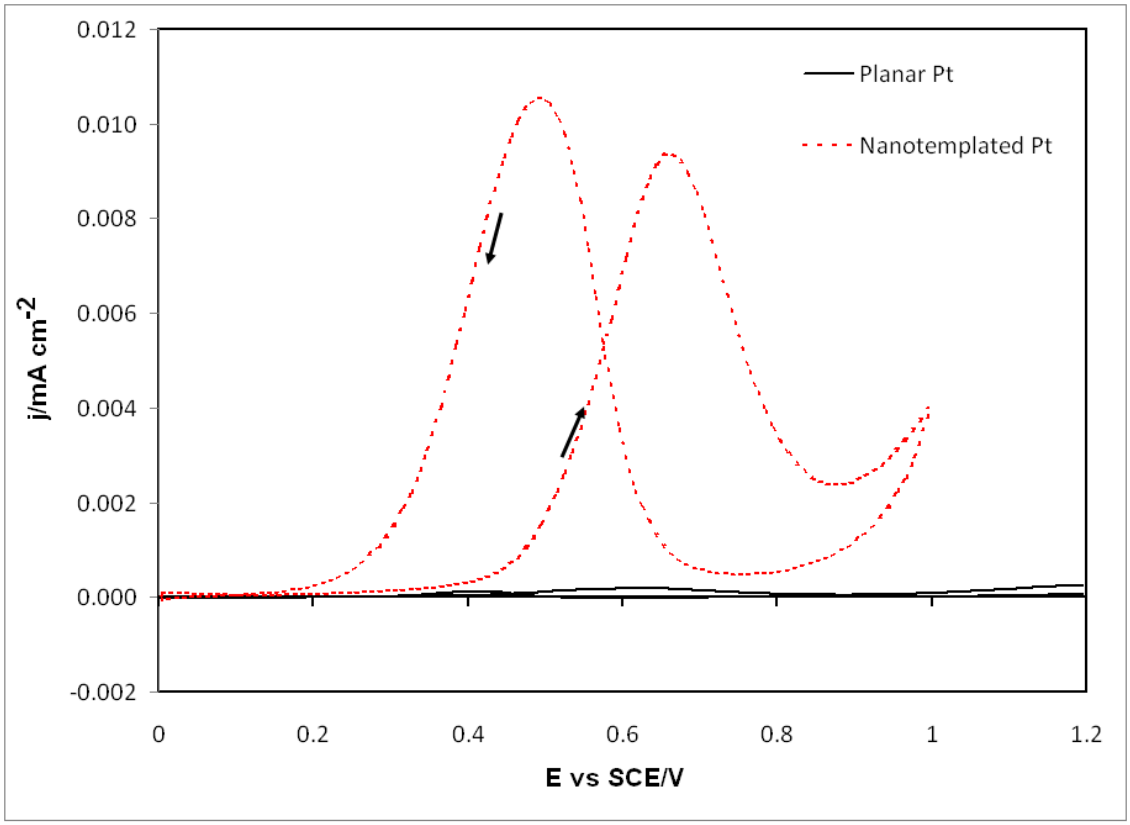

Figure 3. Cyclic voltammograms for 1 mol dm^{-3} CH_3OH in 1 mol dm^{-3} H_2SO_4 at 20°C and 20 mV/s. The working electrodes were nanotemplated Pt (- - -) catalyst fabricated in AAO on Si and planar Pt (——) on Si.

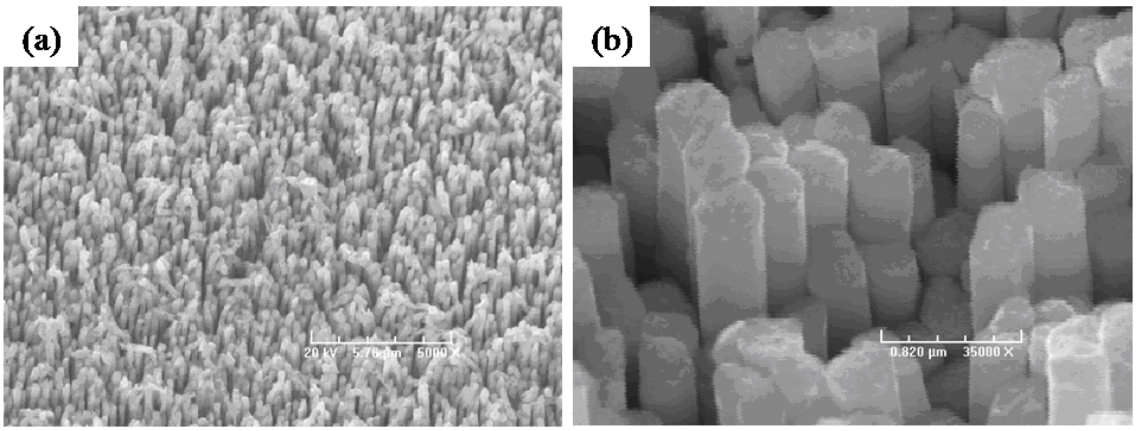

Figure 4: SEM images of templated Cu_6Sn_5 (a) 5000X (b) 35000X magnification.

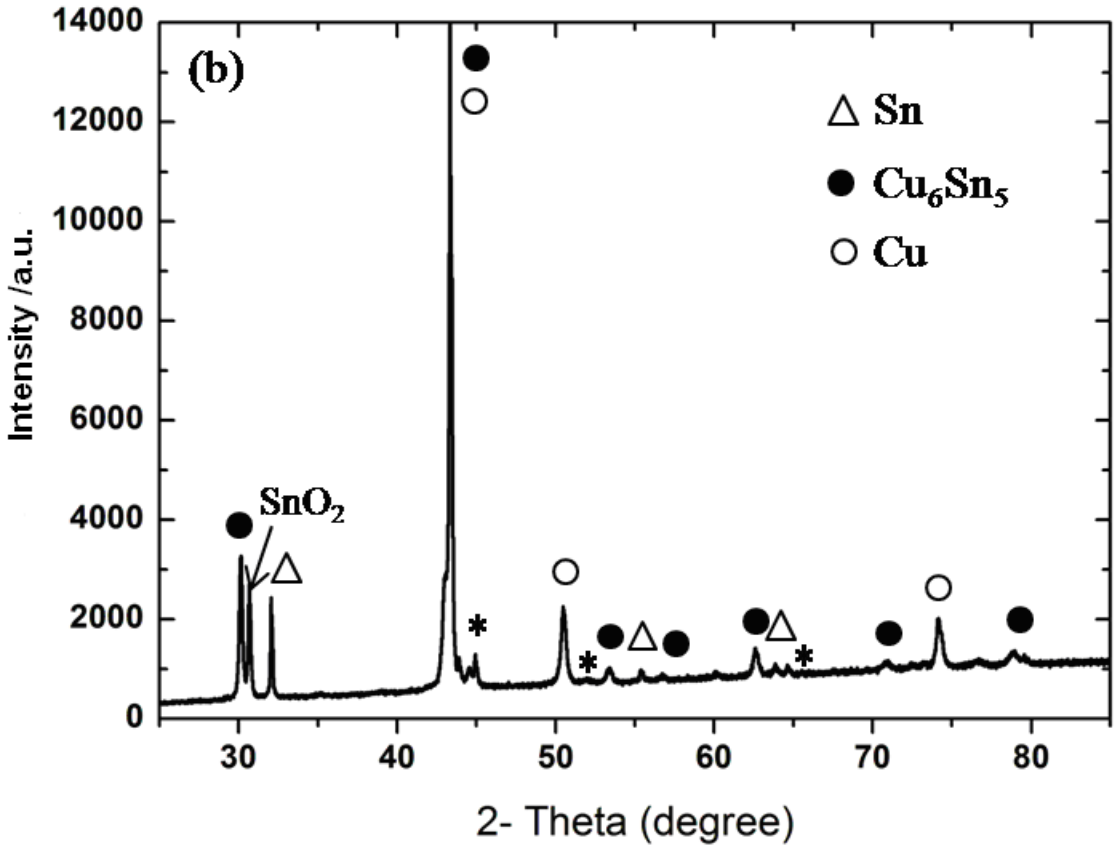

Figure 5. XRD patterns of AAO templated Cu_6Sn_5 deposits. The peaks indicated by asterisks in XRD patterns correspond to Ni evaporated substrate.

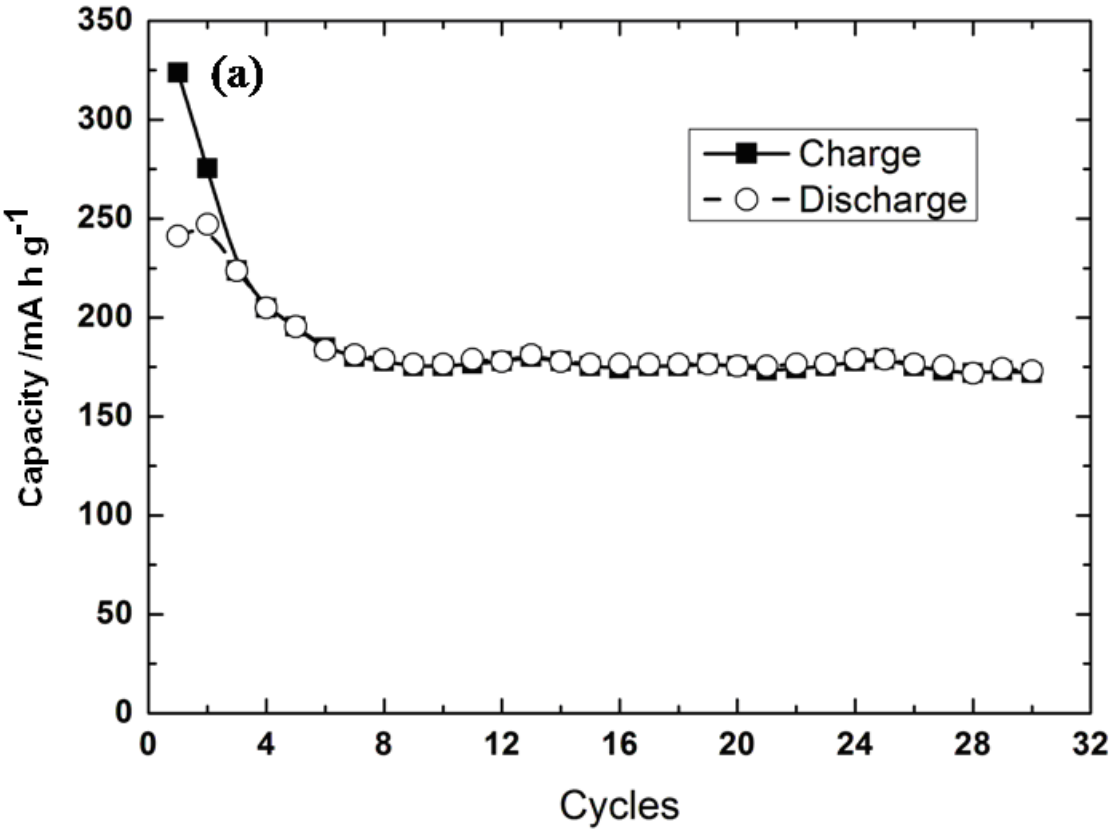

Figure 6. Charge-discharge capacity vs. cycle number for templated Cu_6Sn_5 deposits for 30 cycles.

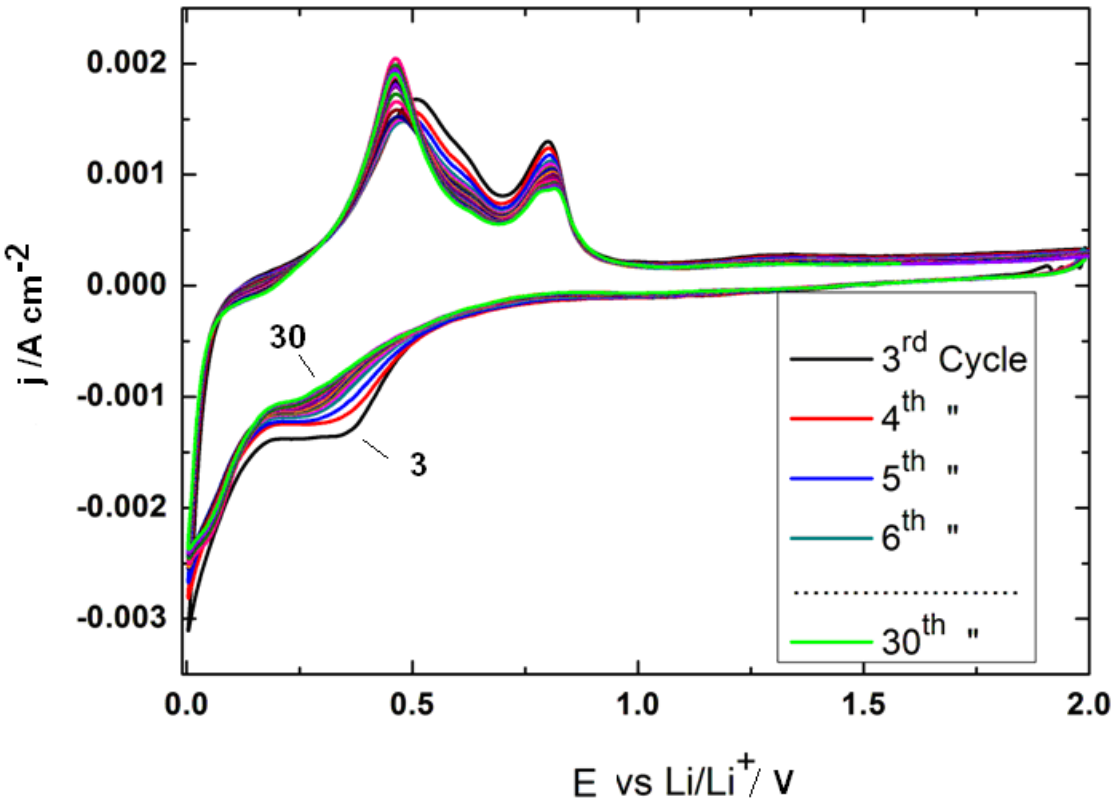

Figure 7: Typical cyclic voltammograms of templated Cu_6Sn_5 deposits from the 3rd cycle (Conditioning/initial potential: 2.0 V, 20 s; scan rate: 0.5 mV/s).